Control System of the Beam-Waveguide Antenna Subreflector: Current Performance and Proposed Upgrades

W. Gawronski[1] and A. Sehic[1]

The article presents the development of the subreflector model of a beam-waveguide antenna, starting from the mechanical hardware, proceeding into the rate-loop system, and finally into the position-loop system. The rate-loop model and the position-loop model simulation results were verified with the field data. The analysis showed that the subreflector displays a nonlinear behavior when excited by larger step offsets (2 mm or larger) and that its bandwidth is identical to the bandwidth of the 70-m antenna subreflector. In order to improve the subreflector dynamics, we propose to increase motor power (e.g., replace a single motor with three motors) or to modify the controller algorithm by adding a feedforward loop and a command preprocessor.

I. Introduction

The purpose of this article is to analyze open- and closed-loop responses of the beam-waveguide (BWG) antenna subreflector servo, to compare them with the field data, to evaluate the servo performance, and to propose design changes to improve the subreflector performance.

In order to accomplish the above goals, we developed the mathematical model of the mechanical part (the subreflector dish, reducers, shafts, and motor), and the obtained differential equations were used to develop the Simulink model of the rate-loop system. The accuracy of the rate-loop system was verified by comparing the simulation results with the data obtained from the rate-loop tests. Eventually we developed the position-loop model of the subreflector, simulated the step responses and rate-offset responses, and compared the simulation results with the field data.

The simulation results were close to the field data, and they showed that the position-loop bandwidth is low and that the servo displays nonlinear behavior in responses to larger steps (2.5 mm or more). The reason for the low bandwidth and nonlinear behavior is the low acceleration limit. The limit depends on the motor power, and to increase the limit one needs to increase motor power.

We propose two modifications of the subreflector to improve its performance. The first modification requires increased gains of the proportional and integral (PI) controller and a more powerful motor.

[1] Communications Ground Systems Section.

The research described in this publication was carried out by the Jet Propulsion Laboratory, California Institute of Technology, under a contract with the National Aeronautics and Space Administration.

The second modification requires a controller upgrade, namely, the addition of the feedforward loop and command preprocessor to the controller. This modification requires software changes only.

II. Open-Loop Model

The subreflector model is shown in Fig. 1. It consists of a (1) motor, (2) worm reducer with drive shaft, (3) ball-screw actuator, and (4) subreflector dish. The equations are derived for each subsystem and consequently combined into the subreflector mechanical model. The final products are the state–space equations of the subreflector model, as presented in Fig. 1. The parameters of the subreflector and its components are given in the Appendix.

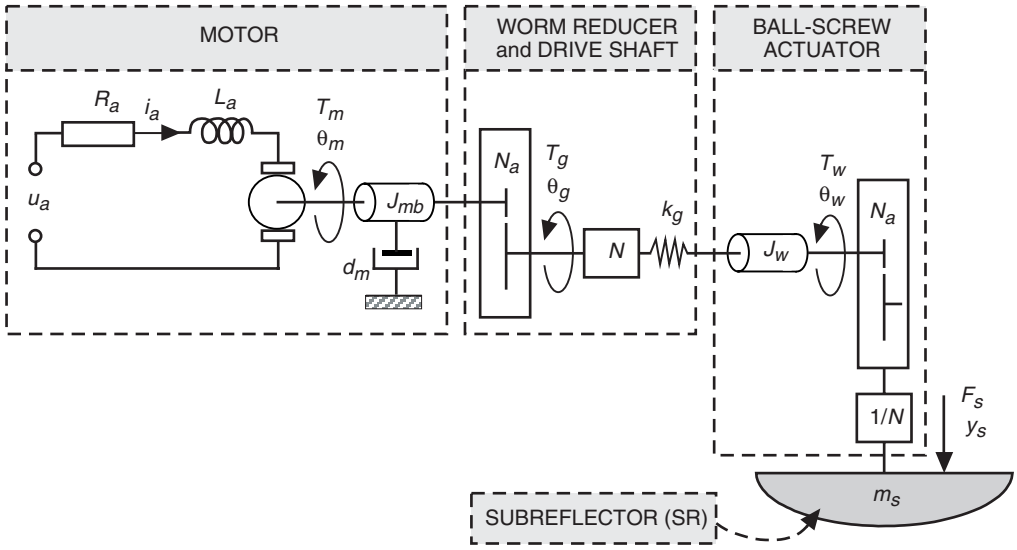

Fig. 1. The subreflector model.

A. Motor Equations

The motor position, θ_m, is controlled by the armature voltage, u_a:

$$u_a = L_a \frac{di_a}{dt} + R_a i_a + k_b \dot{\theta}_m \tag{1}$$

where R_a is motor resistance, L_a is motor inductance, and k_b is the armature constant. The motor torque, T_m, is proportional to the motor current, i_a:

$$T_m = k_t i_a \tag{2}$$

where k_t is the motor-torque constant. The motor torque, T_m, is in equilibrium with the remaining torque acting on the rotor; therefore,

$$T_m = J_{mb} \ddot{\theta}_m + d_m \dot{\theta}_m + T_g \tag{3}$$

and

$$J_{mb} = J_m + J_b \tag{4}$$

is a total inertia of the motor, J_m, and the brake, J_b.

B. Worm Reducer and Drive Shaft Equations

In Eq. (3), T_g is the torque at the output of the gearbox, which can be expressed with the torsional deformation of the gearbox:

$$T_g = \frac{N k_g}{N_g}(\theta_g - \theta_w) \tag{5}$$

and T_g is the torque caused by the drive torsional elastic deformation. Since the reducer has three drive shafts, the total torque is the triple of the individual shaft torque, i.e., the torque is multiplied by $N = 3$; θ_m is the angle of rotation of the motor shaft; d_m is motor viscous damping; k_g is the stiffness of the universal joint, drive shaft, and coupling; N_g is the worm-reducer gear ratio; θ_g is the angle of rotation of the worm-reducer output shaft,

$$\theta_g = \frac{\theta_m}{N_g} \tag{6}$$

and θ_w is the angle of rotation of the ball-screw actuator.

C. Ball-Screw Actuator Equations

The angle of rotation of the ball-screw actuator, θ_w, and the linear displacement of the actuator, y_s, are related through the actuator ratio N_a:

$$\theta_w = N_a y_s \tag{7}$$

where y_s is the subreflector displacement. From Fig. 1, the torques at the ball-screw actuator can be written as

$$J_w \ddot{\theta}_w + k_g(\theta_w - \theta_g) + T_w = 0 \tag{8}$$

where J_w is the inertia of the coupling and the ball-screw actuator, and T_w is the actuator torque.

D. Subreflector Dish Equations

The actuator torque, T_w, is obtained from the subreflector force, F_s, as follows:

$$T_w = \frac{F_s}{N\,N_a} \tag{9}$$

Above, the force is divided by $N = 3$ because the subreflector is moved by three actuators. The force, F_s, is the subreflector inertia force,

$$F_s = m_s \ddot{y}_s \tag{10}$$

where m_s is the mass of the subreflector.

E. Equations of the Entire Subreflector

The above-derived equations allow for writing the dynamics of the entire subreflector. Namely, by introducing Eqs. (6), (7), and (2) into Eq. (3), one obtains

$$k_t i_a = J_{mb}\ddot{\theta}_m + d_m\dot{\theta}_m + \frac{N k_g}{N_g^2}\theta_m - \frac{k_g N\, N_a}{N_g} y_s \tag{11}$$

and by introducing Eqs. (9), (10), (7), and (6) into Eq. (8), one obtains

$$J_w N_a \ddot{y}_s + k_g N_a y_s - \frac{k_g}{N_g}\theta_m + \frac{m_s}{N\, N_a}\ddot{y}_s = 0$$

which can be re-written as follows:

$$(J_w N\, N_a^2 + m_s)\ddot{y}_s + k_g N\, N_a^2 y_s - \frac{k_g N\, N_a}{N_g}\theta_m = 0 \tag{12}$$

Next, we write the above equations in the state–space form, i.e., as a set of the first-order differential equations:

$$\left.\begin{aligned} \dot{x}_s &= A_s x_s + B_s u_a \\ y_o &= C_s x_s \end{aligned}\right\} \tag{13}$$

They are obtained as follows: We define new variables, $\omega_m = \dot{\theta}_m$ (motor velocity) and $v_s = \dot{y}_s$ (subreflector velocity), and re-write Eqs. (11), (12), and (1) as a set of first-order differential equations:

$$\left.\begin{aligned} \dot{\theta}_m &= \omega_m \\ \dot{\omega}_m &= \frac{1}{J_{mb}}\left(-\frac{k_g N}{N_g^2}\theta_m - d_m\omega_m + \frac{k_g N\, N_a}{N_g} y_s + k_t i_a\right) \\ \dot{y}_s &= v_s \\ \dot{v}_s &= \frac{1}{J_w N\, N_a^2 + m_s}\left(\frac{k_g N\, N_a}{N_g}\theta_m - k_g N\, N_a^2 y_s\right) \\ \frac{di_a}{dt} &= \frac{1}{L_a}\left(-k_b\omega_m - R_a i_a + u_a\right) \end{aligned}\right\} \tag{14}$$

Next we define the state variable, x_s, in the state equation, Eq. (13),

$$x_s^T = \{\, \theta_m \quad \omega_m \quad y_s \quad v_s \quad i_a \,\} \tag{15}$$

define the input in Eq. (13) as the voltage, u_a, and the output in Eq. (13) that consists of four variables,

$$y_o^T = \{\, \omega_m \quad y_s \quad v_s \quad i_a \,\} \tag{16}$$

With the above definitions, one obtains the state–space equations, Eq. (13), where the matrices A_s, B_s, and C_s are as follows:

$$A_s = \begin{bmatrix} 0 & 1 & 0 & 0 & 0 \\ -\dfrac{k_g N}{J_{mb} N_g^2} & -\dfrac{d_m}{J_{mb}} & \dfrac{k_g N\, N_a}{J_{mb} N_g} & 0 & \dfrac{k_t}{J_{mb}} \\ 0 & 0 & 0 & 1 & 0 \\ \dfrac{k_g N\, N_a}{N_g (J_w N\, N_a^2 + m_s)} & 0 & -\dfrac{k_g N\, N_a^2}{J_w N\, N_a^2 + m_s} & 0 & 0 \\ 0 & -\dfrac{k_b}{L_a} & 0 & 0 & -\dfrac{R_a}{L_a} \end{bmatrix} \tag{17}$$

$$B_s = \begin{bmatrix} 0 \\ 0 \\ 0 \\ 0 \\ \dfrac{1}{L_a} \end{bmatrix} \tag{18}$$

and

$$C_s = \begin{bmatrix} 0 & 1 & 0 & 0 & 0 \\ 0 & 0 & 1 & 0 & 0 \\ 0 & 0 & 0 & 1 & 0 \\ 0 & 0 & 0 & 0 & 1 \end{bmatrix} \tag{19}$$

The above state–space representation (A_s, B_s, C_s) represents the open-loop subreflector model.

III. Rate-Loop Model

The Simulink model of the rate-loop is shown in Fig. 2. The rate-loop model is obtained from the open-loop model by closing the tachometer feedback loop, where the feedback voltage, u_{af}, is proportional to the tachometer speed,

$$u_{af} = k_{\text{tach}} k_{\text{tach2}} \omega_m \tag{20}$$

The gain k_{tach} relates the tachometer speed with its voltage. The speed of 1 rad/s produces voltage of 0.3 V; therefore, $k_{\text{tach}} = 0.30$ V/rad/s. The gain k_{tach2} represents the scaling of the tachometer voltage range from ± 34.29 V to the subreflector voltage range of ± 10 V; thus, $k_{\text{tach2}} = 10/34.29 = 0.2916$ V/V. The rate loop is closed with the rate-loop proportional gain, k_{rate}. This gain is $k_{\text{rate}} = 1.5$.

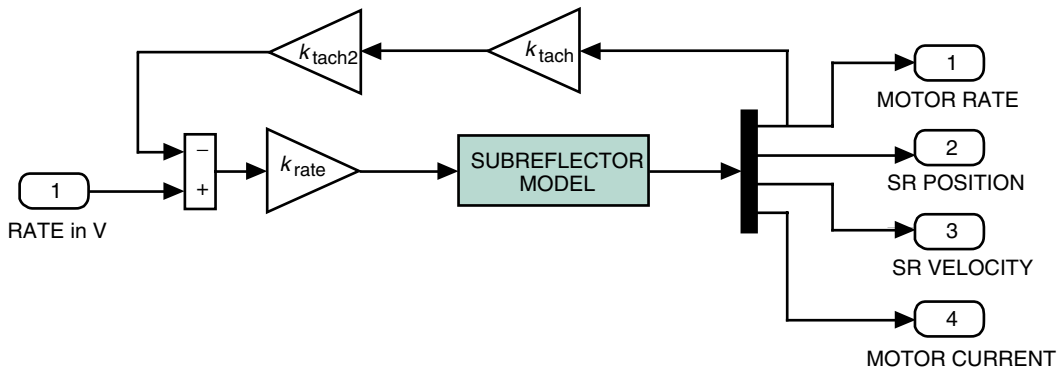

Fig. 2. The rate-loop model.

The response of the rate-loop model to 1-V step input was simulated (in the Simulink model, Fig. 2, it is input 1, called "rate in V"). The step is measured at the motor rate (in the Simulink model, Fig. 2, it is output 1, called "motor rate"). The response is shown in Fig. 3. From this figure, the settling time is 0.14 s, and it is consistent with the rate-loop tests.[2]

The rate-loop transfer function (from rate-voltage input to motor-rate output) is shown in Fig. 4. The plot shows that the rate-loop bandwidth is 4.5 Hz.

IV. Position-Loop Model and Performance

The block diagram of the position-loop control of the subreflector is shown in Fig. 5. It consists of

(1) The rate-loop system, as shown in Fig. 2

(2) The PI controller

(3) Rate and acceleration (ACC) limiters

(4) A gain that scales the rate command into the voltage command

The PI controller gains are as follows: the proportional gain is $k_p = 2.0$, and the integral gain is $k_i = 0.5$. The scaling factor from the rate command to the voltage command is $k_{rv} = 7874$ V s/m. The rate limit is $v_{\max} = 1.27 \times 10^{-3}$ m/s (or 3 in./min), and the acceleration limit is $a_{\max} = 7.0556 \times 10^{-4}$ m/s^2 (or 100 in./min^2).

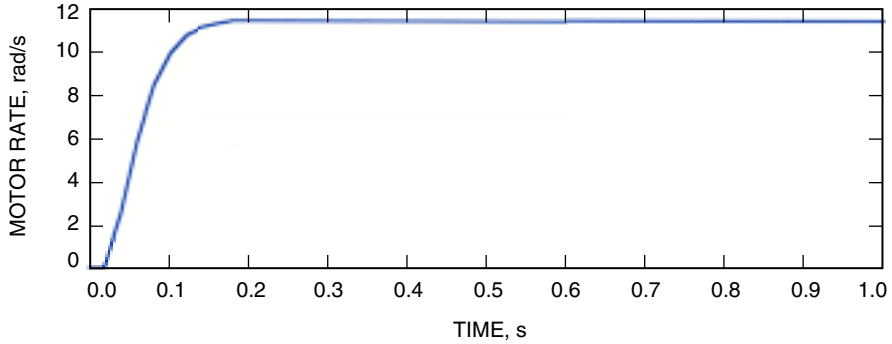

Fig. 3. The motor-rate response to 1-V step input.

[2] W. Gawronski, "Open-Loop Tests of the BWG Antenna Subreflector," JPL Memorandum (internal document), Jet Propulsion Laboratory, Pasadena, California, December 20, 2002.

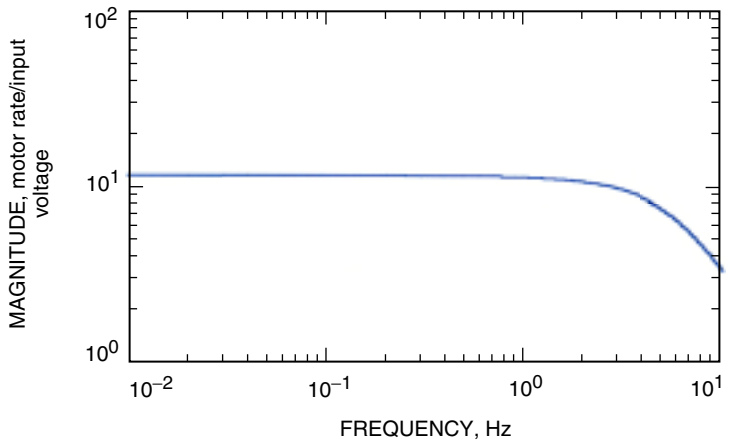

Fig. 4. The rate-loop transfer function: from the rate-voltage input to the motor-rate output.

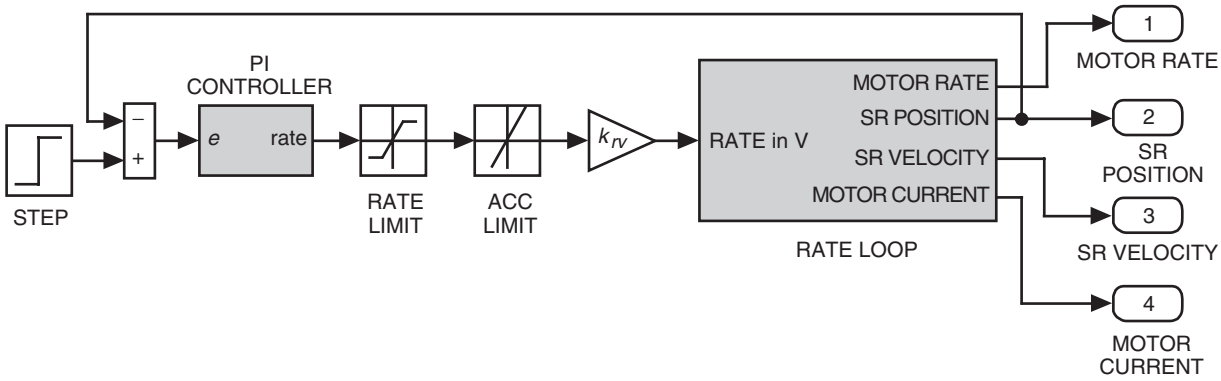

Fig. 5. The position-loop model.

In order to evaluate the servo performance, the transfer function of the position-loop model (from the subreflector position command to the subreflector actual position) was obtained and shown in Fig. 6. The plot shows that the position-loop bandwidth is 0.35 Hz. The bandwidth is comparatively low, and it can be increased by changing the controller gains (although it might also require the increase of the motor power, as we will discuss later).

Next, the subreflector simulations were conducted to compare the simulation results with the available field data. The position-loop tests were conducted by Bill Almassy in 1994, as has been reported.[3] They include measurements of the subreflector responses to position and rate offsets in the y- and z-directions. Here we compare the position offsets of 0.5 mm and 2.5 mm, and the rate offsets of 0.025 mm/s in the z-direction. The plots of the responses of the subreflector to the 0.5-mm offset are shown in Fig. 7(a) (simulated results) and Fig. 7(b) (field data), and plots of the responses of the subreflector to the 2.5-mm offset are shown in Fig. 8(a) (simulated results) and Fig. 8(b) (field data). The simulation and field data are not exactly the same due to some uncertainty in the subreflector data model; however, they represent a satisfactory accuracy at this stage of analysis. Note that the 0.5-mm step response and 2.5-mm step response are not similar (although they should be if the system were linear). The excessive overshoot and undershoot are due to the fact that the system hit the rate and acceleration limits for the step of

[3] W. Gawronski, "Closed-Loop Tests of the DSS24 Antenna Subreflector," JPL Interoffice Memorandum (internal document), Jet Propulsion Laboratory, Pasadena, California, December 20, 2002.

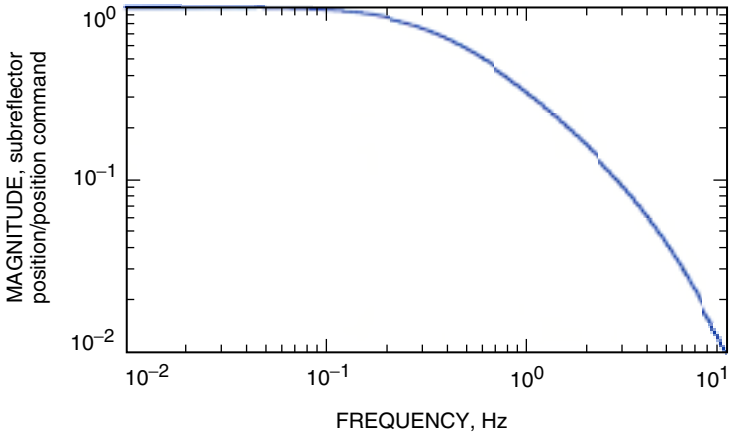

Fig. 6. The position-loop transfer function: from the position command to the subreflector position.

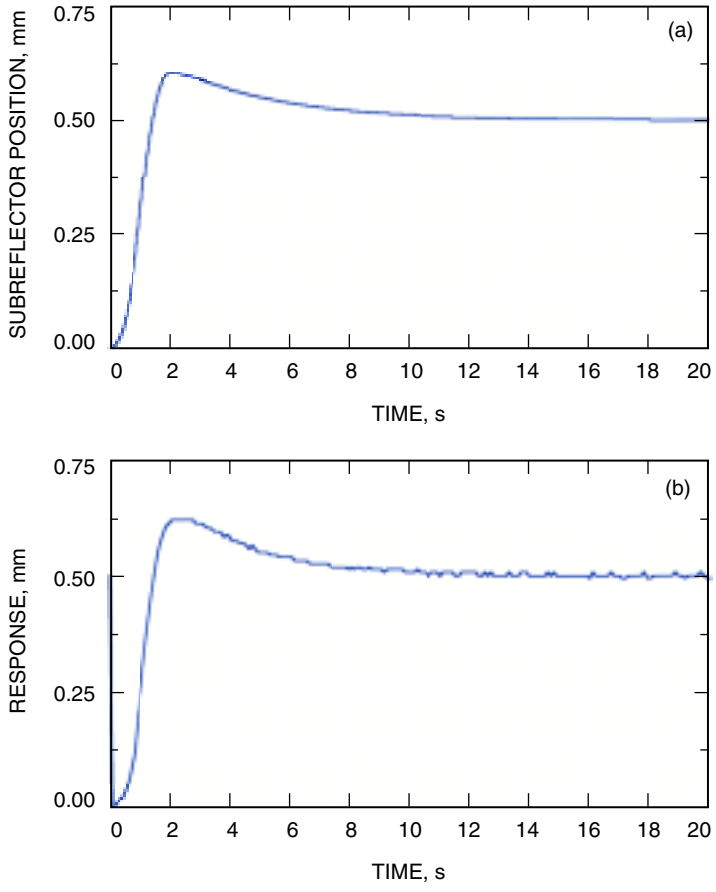

Fig. 7. Responses to 0.5-mm step: (a) simulation results and (b) field data.

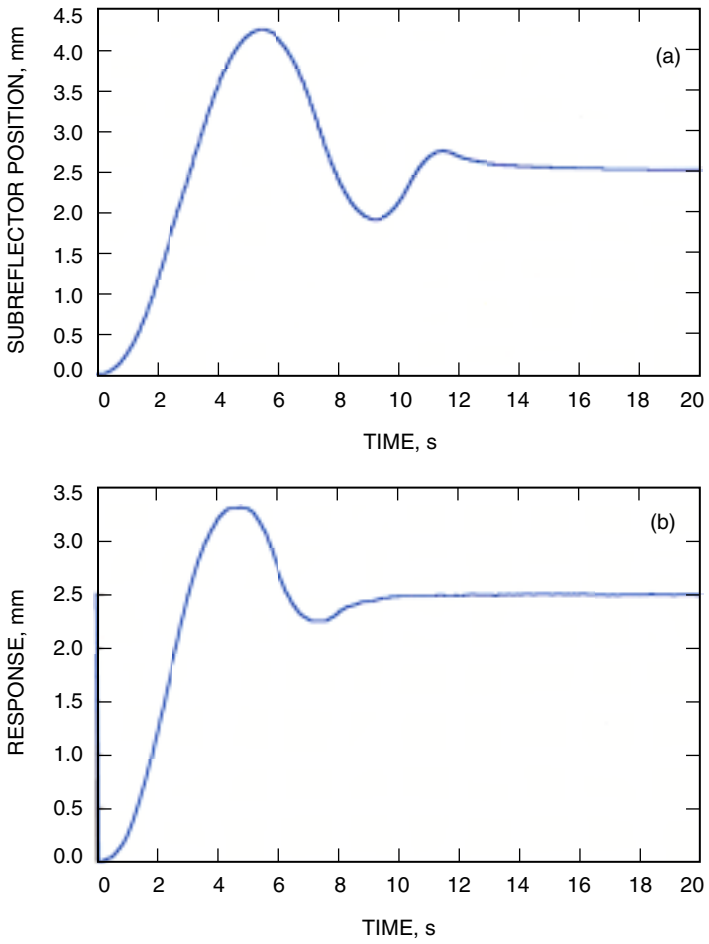

Fig. 8. Responses to 2.5-mm step: (a) simulation results and (b) field data.

2.5 mm. Indeed, the simulation results in Figs. 9(a) and 9(b) show the rate and acceleration saturation of the control signal (just after the rate and acceleration limiters).

This nonlinear behavior is due to low acceleration limits applied to the subreflector servo. These limits are the result of the low motor power. The acceleration limits also can be blamed for the low bandwidth of the position-loop system (which is lower than the 70-m antenna subreflector).

Next, in Fig. 10 we compared the servo errors created by the rate offset of 0.025 mm/s in the z-axis. Figure 10(a) shows the simulated results, while Fig. 10(b) shows the field data. The simulation shows smaller servo error.

Finally, we simulate typical subreflector movements that change with the elevation position of the antenna. Consider y-axis movement. The y-position for the DSS-26 antenna depends on the antenna elevation position as follows:[4]

$$y = -5.19\big(\sin(45^\circ) - \sin(EL)\big) - 52.20\big(\cos(45^\circ) - \cos(EL)\big) \tag{21}$$

[4] Data from D. Rochblatt, Jet Propulsion Laboratory, Pasadena, California, March 3, 2003.

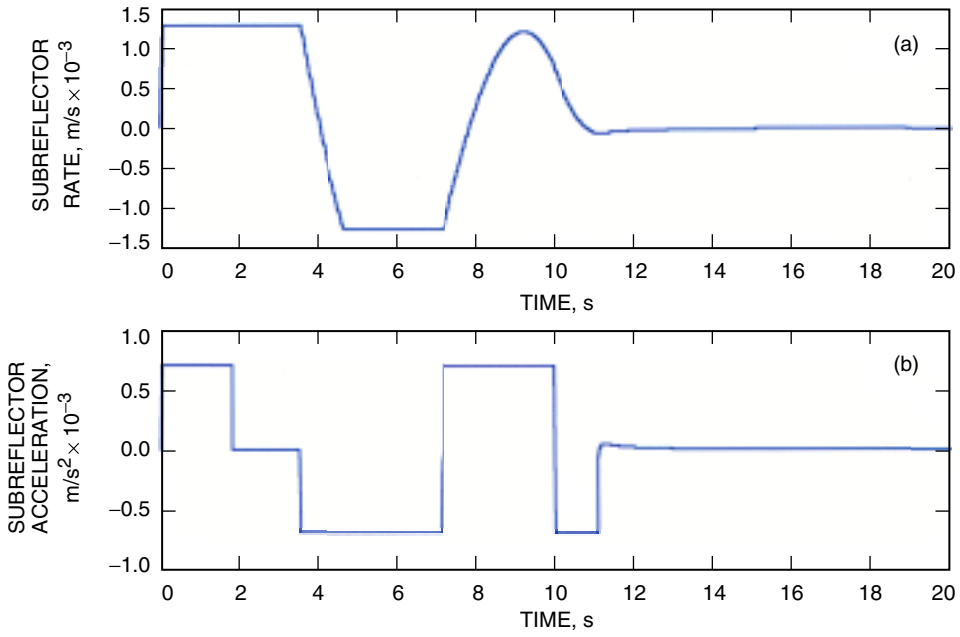

Fig. 9. The subreflector (a) velocity and (b) acceleration for 2.5-mm step.

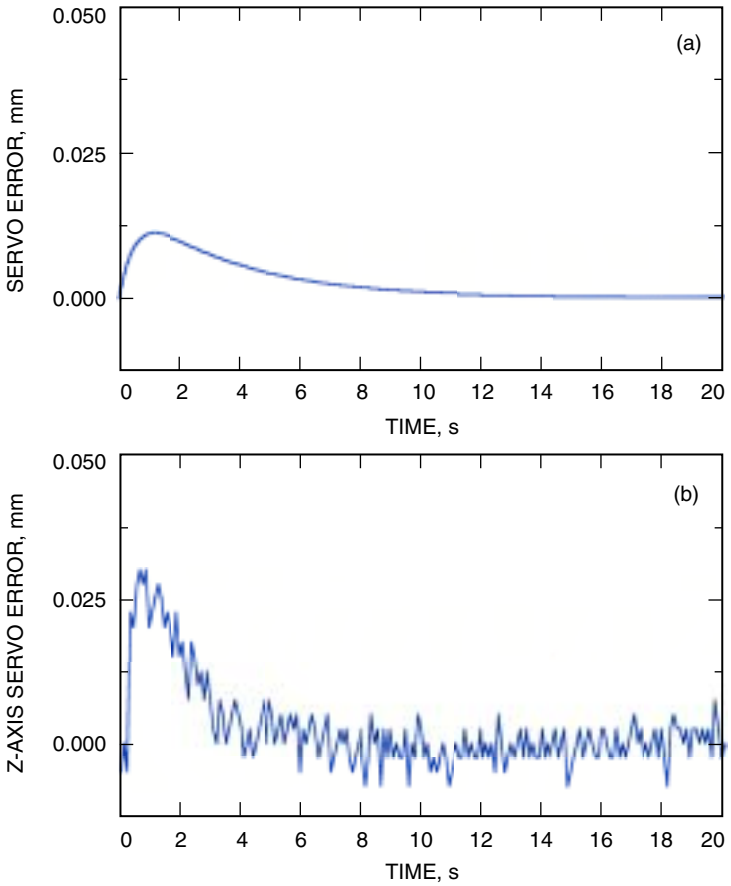

Fig. 10. The servo error for the 0.025-mm/s rate offset: (a) simulation results and (b) field data.

where EL is the antenna elevation position in deg and y is in mm. Assume now that the antenna is at the 44-deg elevation position and will move to the 13-deg position at its maximal rate of 0.8 deg/s, where it starts tracking at the rate of 0.005 deg/s. The plot of antenna movement is shown in Fig. 11 (dashed line). The subreflector will move according to Eq. (21), and its movement also is shown in Fig. 11 (solid line). The subreflector tracking error (a difference between command and the actual subreflector position) is shown in Fig. 12. The figure shows that, after transient motion, the subreflector steady-state error is 0.02 mm for the fast movement and 0 mm for "normal" tracking. This example shows that the subreflector servo satisfies the tracking requirement.

V. Proposed Improvements of the Servo Performance

There is observed nonlinear behavior of the position-loop servo. It still allows the servo to reach the commanded position, but with excessive overshoots. We investigated two ways to improve the servo performance: by hardware modifications and by software modifications.

The hardware modifications include the increase of the PI controller gains. The current gains are

Proportional gain: $k_p = 2$

Integral gain: $k_i = 0.5$

And we propose the following gains:

Proportional gain: $k_p = 4$

Integral gain: $k_i = 3$

This modification will decrease the settling time from 10 s to 4 s and increase the bandwidth from 0.35 Hz to 0.9 Hz. This can be seen by comparing the step responses of the current system [Fig. 7(a)] and the improved system (Fig. 13), and by comparing the magnitudes of the transfer function of the current system (Fig. 6) and the improved system (Fig. 14). The improvement, however, will require raising the rate and acceleration limits by a factor of 5 (at least) and, consequently, applying a more powerful motor, or three motors instead of one.

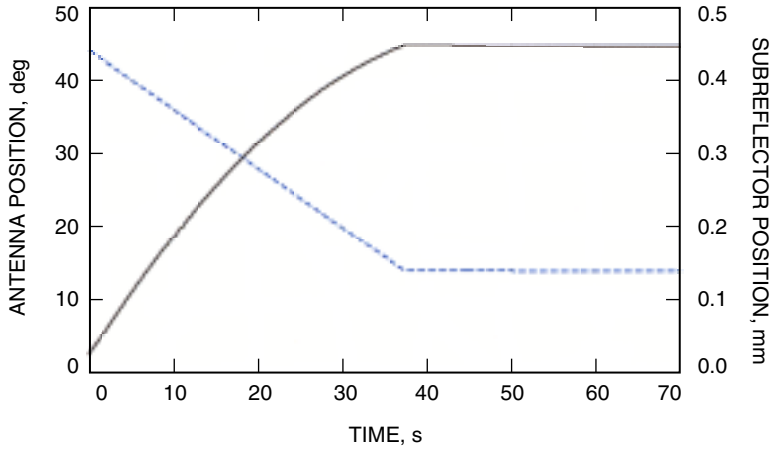

Fig. 11. The antenna movement (dashed line) and the corresponding subreflector position (solid line).

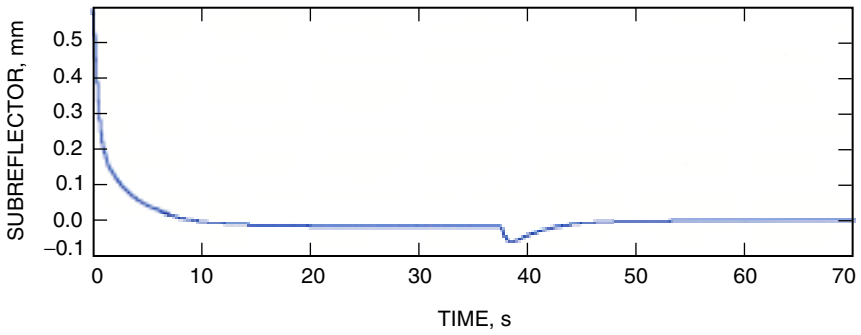

Fig. 12. The subreflector tracking error.

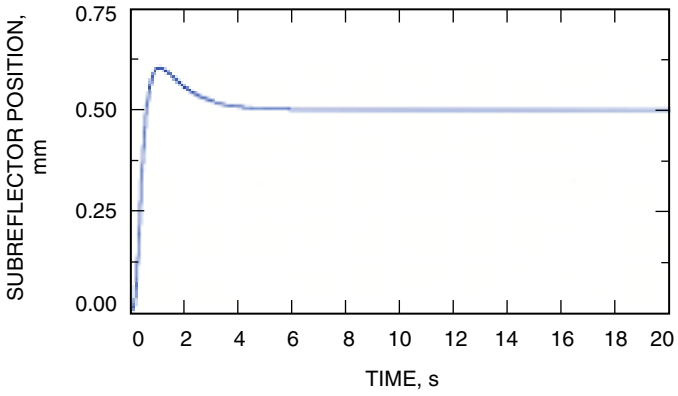

Fig. 13. The step response of the improved servo.

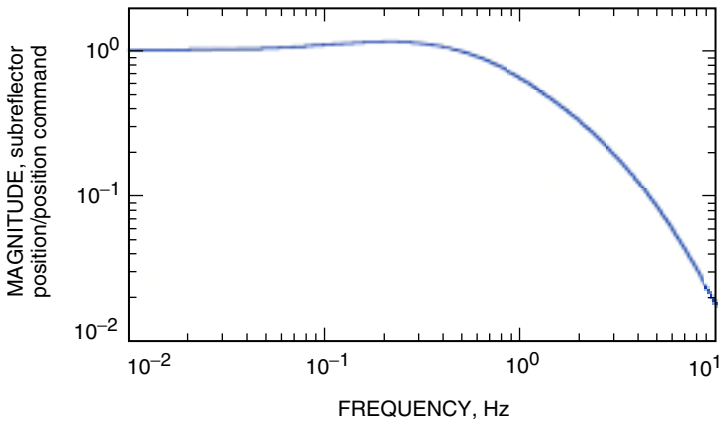

Fig. 14. The transfer function of the improved servo: from the position command to the subreflector position.

The second modification would require changes of the control law, including the addition of a feedforward loop and the command processor. These modifications would require software changes only and are shown in Fig. 15. The command preprocessor (CPP) is described in [2] and [3], and its parameters for this subreflector are as follows: $\beta = 200$, $k_o = 0$, and $k_v = 1$.

The step responses of the modified system are shown in Fig. 16(a) for the small step (0.5 mm) and in Fig. 16(b) for the larger step (2.5 mm). They do not have overshoot, and the settling time is less than 4 s.

The tracking properties of the modified servo were tested with the 0.025-mm/s rate offset. The servo error for this tracking is shown in Fig. 17. The steady-state error is zero, and the maximal error is 0.0023 mm, while for the current servo it is 0.0117 mm (simulated) and 0.0234 mm (measured), showing that the modified servo has the smallest tracking error.

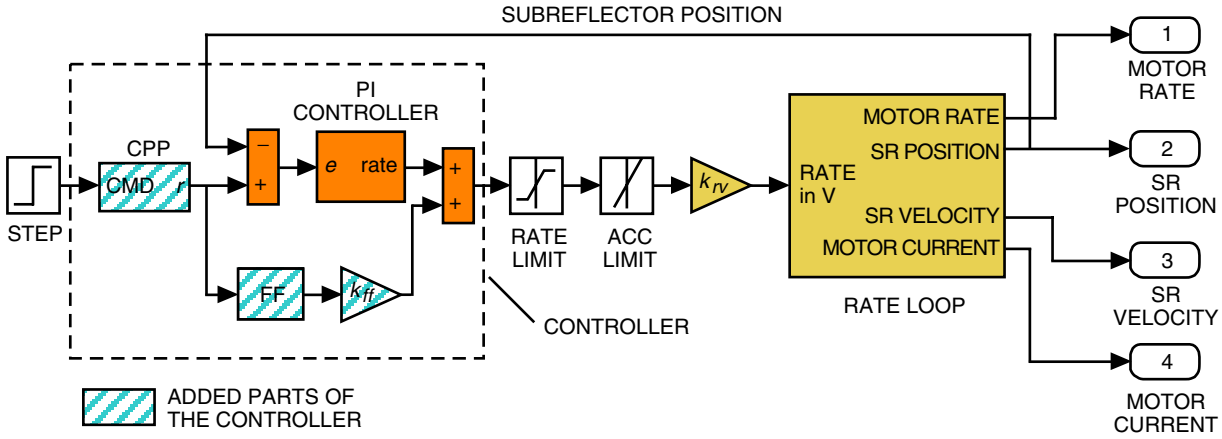

Fig. 15. The modified position-loop model.

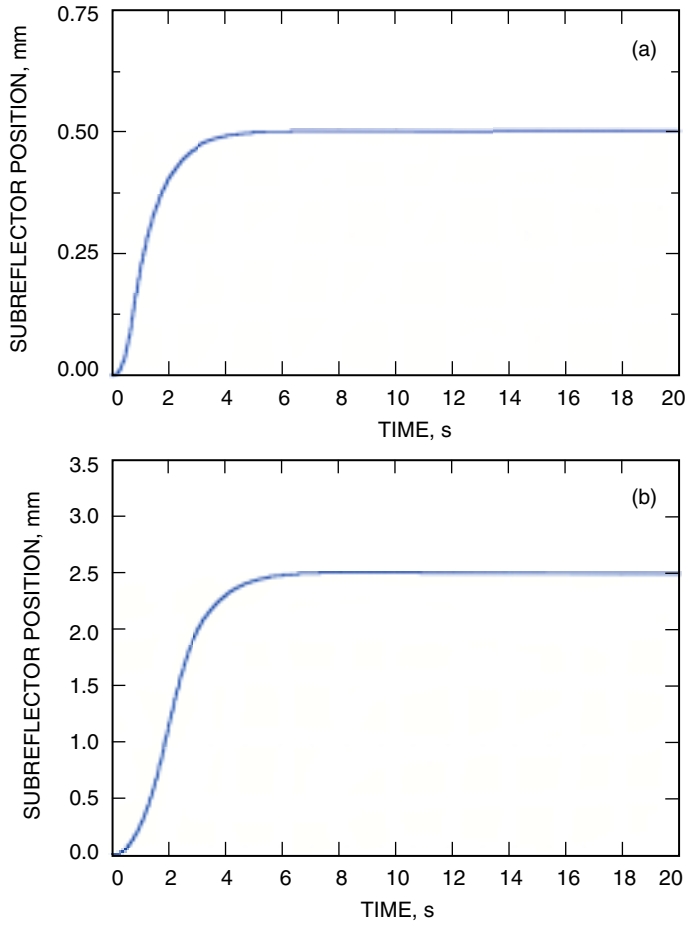

Fig. 16. The step responses of the modified servo: (a) 0.5-mm step and (b) 2.5-mm step.

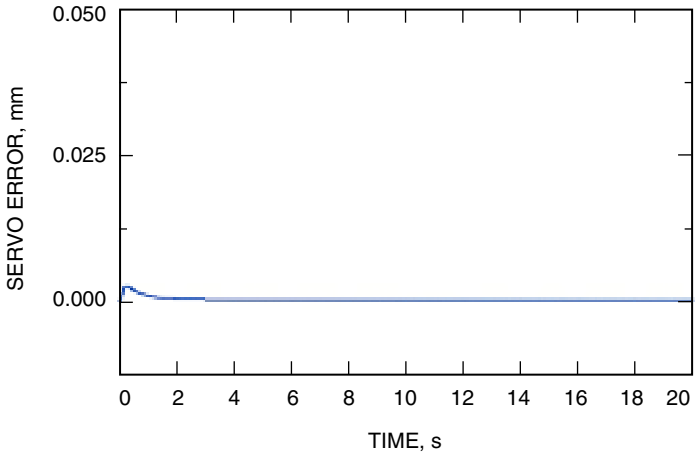

Fig. 17. The servo error of the modified servo for the 0.025-mm/s rate offset.

VI. Conclusions

The subreflector servo model was developed, and the simulations were conducted. Their results were compared with field data. The simulation results are close enough to reflect the important properties of the subreflector servo.

Comparing the BWG subreflector with the DSS-14 subreflector (cf., [1]), one can see that the BWG servo is slower and has lower bandwidth. We propose two modifications of the subreflector to improve the performance. The first modification requires a more powerful motor and increased gains of the PI controller. The second modification requires the addition of the feedforward loop and command preprocessor to the controller. This modification requires a software change only.

References

[1] F. Baher, "Open- and Closed-Loop Analysis of the 70-Meter Antenna Subreflector Positioner," *The Telecommunications and Mission Operations Progress Report 42-145, January–March 2001*, Jet Propulsion Laboratory, Pasadena, California, pp. 1–15, May 15, 2001.
http://tmo.jpl.nasa.gov/tmo/progress_report/42-145/145B.pdf

[2] W. Gawronski, "Command Preprocessor for the Beam-Waveguide Antennas," *The Telecommunications and Mission Operations Progress Report 42-136, October–December 1998,* Jet Propulsion Laboratory, Pasadena, California, pp. 1–10, February 15, 1999.
http://tmo.jpl.nasa.gov/tmo/progress_report/42-136/136A.pdf

[3] W. Gawronski, and W. Almassy, "Command Pre-Processor for Radiotelescopes and Microwave Antennas," *IEEE Antennas and Propagation Magazine,* vol. 44, pp. 30–37, 2002.

Appendix
Subreflector Data

$R_a = 0.59\Omega$	Motor resistance
$L_a = 0.00552$ H	Motor inductance
$J_m = 0.00452$ kg m^2	Motor inertia (0.04 lbf in. s^2)
$J_b = 0.004$ kg m^2	Brake inertia
$J_w = 0.00336$ kg m^2	Inertia of coupling and ball-screw actuator, Eq. (8)
$d_m = 4.52 \times 10^{-4}$ N m s/rad	Motor damping, Eq. (3) (0.004 lbf in./rad/s)
$N = 3$	Number of actuators
$N_g = 7.5$	Worm-reducer gear ratio
$Na = 1.2531 \times 10^4$ rad/m	Actuator ratio (50.66 rev/in.)
$m_s = 492$ kg	Subreflector mass (1082 lb)
$k_g = 10,092$ N m/rad	Stiffness of the drive shaft
$k_t = 0.3954$ Nm/A	Motor-torque constant, Eq. (2) (3.50 lb in./A)
$k_b = 0.40 \times 0$ V/rad/s	Armature constant, Eq. (1)
$k_{\text{tach}} = 0.30$ V/rad/s	Tachometer gain
$k_{\text{tach2}} = 0.2916$ V/V	Tachometer voltage scaling factor
$k_{\text{rate}} = 1.5$	Rate-loop gain
$k_{rv} = 7874$ V s/m	Rate-to-volts gain (10 V = 3 in./min)
$k_p = 2.0$	Proportional gain
$k_i = 0.5$	Integral gain
$v_{\max} = 1.27 \times 10^{-3}$ m/s	Rate limit (3 in./min)
$a_{\max} = 7.0556 \times 10^{-4}$ m/s^2	Acceleration limit (100 in./min^2)